AIAA Aviation
22-26 June 2015, Dallas, TX
7th AIAA Atmospheric and Space Environments Conference

Well-Balanced Formulation of Gravitational Source Terms for Conservative Finite-Difference Atmospheric Flow Solvers

Debojyoti Ghosh* and Emil M. Constantinescu †
Argonne National Laboratory, Lemont, IL 60439, United States

Numerical simulation of atmospheric flows requires high-resolution, nonoscillatory algorithms to accurately capture all length scales. In this paper, a conservative finite-difference algorithm is proposed that uses the weighted essentially nonoscillatory and compact-reconstruction weighted essentially nonoscillatory schemes for spatial discretization. These schemes use solution-dependent interpolation stencils to yield high-order accurate nonoscillatory solutions to hyperbolic conservation laws. The Euler equations in their fundamental form (conservation of mass, momentum, and energy) are solved, thus avoiding approximations and simplifications. A well-balanced formulation of the finite-difference algorithm is proposed that preserves hydrostatically balanced equilibria to round-off errors. The algorithm is verified for benchmark atmospheric flow problems.

I. Introduction

Recent decades have seen the development of several numerical algorithms for accurately simulating atmospheric flows. Flows with large horizontal scales are often solved with hydrostatic models[1,2] or simplified models that remove acoustic waves.[3,4,5] High-resolution simulations at smaller length scales need to model nonhydrostatic effects and require the solution of the compressible Euler equations,[6,7,8] of which several formulations have been proposed in the literature.[9,10] Algorithms have been proposed based on expressing the Euler equations in terms of derived quantities that are relevant to atmospheric flows;[11,12,13,14,15] however, these methods do not conserve mass, momentum, and energy. Alternatively, the assumption of adiabaticity simplifies the energy conservation equation to conservation of the potential temperature;[16] and several numerical algorithms are based on this adiabatic form of the Euler equations.[17,18] Some recent efforts have proposed solving the Euler equations as the conservation of mass, momentum, and energy with no simplifying assumptions,[19,20,9,21] thus allowing the conservation of energy to machine precision, as well as specification of the true viscous terms, should they be required. This approach is followed in the present study.

Finite-difference algorithms have been used to simulate atmospheric flows;[17,12,22] however, they have two primary drawbacks: low spectral resolution (due to low-order spatial discretization) and the lack of scalability.[23] High-order finite-volume[8,18,19,21,24] and finite-element or spectral-element[9,10,23] methods have been proposed that address these drawbacks. These flows are often characterized by strong gradients, and linear spatial discretization methods often need an additional filter or artificial diffusion to stabilize the solution.[9] Recent developments in conservative finite-difference methods include weighted essentially nonoscillatory (WENO) schemes[25,26] that use solution-dependent interpolation stencils to yield high-order accurate nonoscillatory solutions. WENO schemes have been applied successfully to several application areas.[27] Flows with multiple-length scales require numerical methods with a high spectral resolution, and compact-reconstruction WENO (CRWENO) schemes[28] improve the spectral resolution of the WENO schemes by applying the solution-dependent interpolation stencil-selection to compact finite-difference schemes.[29] CRWENO schemes have been applied to turbulent flows[30] and aerodynamic flows[31] where the resolution of small-length scales is crucial. A scalable implementation of the CRWENO scheme[32] demonstrated its performance for massively parallel simulations. Thus, the WENO and CRWENO schemes are well suited for simulating atmospheric flows.

The Euler equations with the gravitational terms constitute a hyperbolic balance law, and a crucial aspect of balance laws is that they admit steady states where the flux derivatives are balanced by the source term. In particular, the gravitational body forces are balanced by the pressure gradient for steady-state atmospheric flows. Numerical methods must be able to preserve such steady states on finite grids; errors introduced have the potential to overwhelm the flow, which often is itself a small perturbation around the hydrostatic balance. Several algorithms address this problem by expressing

*Postdoctoral Appointee, Mathematics & Computer Science Division, ghosh@mcs.anl.gov.
†Computational Mathematician, Mathematics & Computer Science Division, emconsta@mcs.anl.gov.

the governing equations in terms of the perturbations of the flow variables over their hydrostatically balanced values.[9,8,24] Alternatively, the governing equations expressed in terms of the total variables are solved with well-balanced methods that preserve the balanced steady state to machine precision. Balanced finite-volume methods have been proposed[33,34] and applied to the Euler equations with gravitational source terms.[19,18,21] A well-balanced finite-difference WENO method for the Euler equations with gravitational terms was proposed recently;[35] however, the method was derived and implemented for the isothermal equilibrium only, and no flow problems relevant to atmospheric flows were considered. In the present study, the high-order well-balanced finite-difference formulation[36,35] is extended to atmospheric flows by deriving a general well-balanced formulation for the Euler equations with gravitational source terms. This formulation is then shown to preserve several examples of the hydrostatic equilibria encountered in atmospheric flows. The balanced formulation for the isothermal equilibrium[35] is shown to be a specific case of the general formulation proposed here.

The outline of the paper is as follows. Section II describes the governing equations. The numerical method, including the well-balanced formulation, is described in Sec. III. The algorithm is verified, and results for benchmark flow problems are presented in Sec. IV. The Appendix contains three examples of the general well-balanced formulation.

II. Governing Equations

Atmospheric flows are governed by the inviscid Euler equations[37] with the addition of gravitational and Coriolis forces, and several formulations exist in the literature.[9,10] The Euler equations stated as the conservation of mass, momentum, and energy are used in this study. Mesoscale flows are considered, but Coriolis forces are neglected. The governing equations are expressed as

$$\frac{\partial \rho}{\partial t} + \nabla \cdot (\rho \mathbf{u}) = 0, \tag{1}$$

$$\frac{\partial (\rho \mathbf{u})}{\partial t} + \nabla \cdot (\rho \mathbf{u} \otimes \mathbf{u} + p \mathcal{I}_d) = -\rho \mathbf{g}, \tag{2}$$

$$\frac{\partial e}{\partial t} + \nabla \cdot (e + p)\, \mathbf{u} = -\rho \mathbf{g} \cdot \mathbf{u}, \tag{3}$$

where ρ is the density, $\mathbf{u}$ is the velocity vector, p is the pressure, and $\mathbf{g}$ is the gravitational force vector (per unit mass). $\mathcal{I}_d$ denotes the identity matrix of size d, where d is the number of space dimensions. The energy is given by

$$e = \frac{p}{\gamma - 1} + \frac{1}{2} \rho \mathbf{u} \cdot \mathbf{u}, \tag{4}$$

where γ is the specific heat ratio. The equation of state relates the pressure, density, and temperature as $p = \rho R T$, where R is the universal gas constant and T is the temperature. Two additional quantities of interest in atmospheric flows are the Exner pressure π and the potential temperature θ, defined as

$$\pi = \left(\frac{p}{p_0} \right)^{\frac{\gamma - 1}{\gamma}}, \text{ and } \theta = \frac{T}{\pi}, \tag{5}$$

respectively. The pressure at a reference altitude is denoted by p_0.

III. Numerical Method

Equations (1)–(3) are discretized by a conservative finite-difference method. Two-dimensional flows with gravitational forces acting along the y dimension are considered in this study, and the governing equations can be expressed as a hyperbolic conservation law,

$$\frac{\partial \mathbf{q}}{\partial t} + \frac{\partial \mathbf{F}(\mathbf{q})}{\partial x} + \frac{\partial \mathbf{G}(\mathbf{q})}{\partial y} = \mathbf{s}(\mathbf{q}), \tag{6}$$

where the state vector, the flux vectors along x and y, and the source terms are

$$\mathbf{q} = \begin{bmatrix} \rho \\ \rho u \\ \rho v \\ e \end{bmatrix}, \ \mathbf{F} = \begin{bmatrix} \rho u \\ \rho u^2 + p \\ \rho u v \\ (e + p) u \end{bmatrix}, \ \mathbf{G} = \begin{bmatrix} \rho v \\ \rho u v \\ \rho v^2 + p \\ (e + p) v \end{bmatrix}, \ \mathbf{s} = \begin{bmatrix} 0 \\ 0 \\ -\rho g \\ -\rho v g \end{bmatrix}. \tag{7}$$

The Cartesian velocity components are u and v, and g is the gravitational force (per unit mass). A conservative spatial discretization[38,39] of Eq. (6) yields a semi-discrete ordinary differential equation (ODE) in time,

$$\frac{d\mathbf{q}_{ij}}{dt} + \frac{1}{\Delta x}\left(\hat{\mathbf{f}}_{i+1/2,j} - \hat{\mathbf{f}}_{i-1/2,j}\right) + \frac{1}{\Delta y}\left(\hat{\mathbf{g}}_{i,j+1/2} - \hat{\mathbf{g}}_{i,j-1/2}\right) = \mathbf{s}_{ij}, \tag{8}$$

where $\mathbf{q}_{ij} = \mathbf{q}(x_i, y_j)$ is the cell-centered solution, $(x_i = i\Delta x, y_j = j\Delta y)$ are the spatial coordinates of a grid point, and i, j denote the grid indices. The numerical approximation to the flux function at the cell interfaces $\hat{\mathbf{f}}_{i+1/2,j}, \hat{\mathbf{g}}_{i,j+1/2}$ satisfy

$$\left.\frac{\partial \mathbf{F}}{\partial x}\right|_{x_i,y_j} = \frac{1}{\Delta x}[\hat{\mathbf{f}}(x_{i+1/2,j}, t) - \hat{\mathbf{f}}(x_{i-1/2,j}, t)] + O\left(\Delta x^r\right), \tag{9}$$

$$\left.\frac{\partial \mathbf{G}}{\partial y}\right|_{x_i,y_j} = \frac{1}{\Delta y}[\hat{\mathbf{g}}(x_{i+1/2,j}, t) - \hat{\mathbf{g}}(x_{i-1/2,j}, t)] + O\left(\Delta y^r\right), \tag{10}$$

for an rth-order spatial discretization method. The discretized source term $\mathbf{s}_j$ in Eq. (8) is expressed as its cell-centered value, and this naive treatment does not preserve the hydrostatic equilibrium.[35] The treatment of the source term for a well-balanced formulation is discussed in subsequent sections.

A. Reconstruction

The reconstruction step approximates the numerical flux $\hat{\mathbf{f}}$ and $\hat{\mathbf{g}}$ at the cell interfaces from the cell-centered flux functions $\mathbf{F}(\mathbf{q})$ and $\mathbf{G}(\mathbf{q})$, respectively. The reconstruction procedure for a one-dimensional function is described in this section; specifically, it involves the approximation of the interface flux $\hat{\mathbf{f}}_{j+1/2} = \hat{\mathbf{f}}\left(x_{j+1/2}\right)$ from a cell-centered flux function $\mathbf{f}_j = \mathbf{f}\left(x_j\right)$ to the desired accuracy. It can be trivially extended to multiple dimensions for computing the approximate flux terms in Eq. (8). The fifth-order WENO[26] and CRWENO[28] schemes are used in this study and are briefly summarized below. This discussion considers a left-biased reconstruction of a scalar flux; the corresponding right-biased reconstruction can be similarly obtained. Vector quantities are reconstructed in a componentwise way.

The fifth-order WENO scheme (WENO5)[26] is constructed by considering three third-order accurate interpolation schemes for the numerical flux $\hat{f}_{j+1/2}$:

$$\hat{f}^1_{j+1/2} = \frac{1}{3}f_{j-2} - \frac{7}{6}f_{j-1} + \frac{11}{6}f_j,\ c_1 = \frac{1}{10}, \tag{11}$$

$$\hat{f}^2_{j+1/2} = -\frac{1}{6}f_{j-1} + \frac{5}{6}f_j + \frac{1}{3}f_{j+1},\ c_2 = \frac{6}{10}, \tag{12}$$

$$\hat{f}^3_{j+1/2} = \frac{1}{3}f_j + \frac{5}{6}f_{j+1} - \frac{1}{6}f_{j+2},\ c_3 = \frac{3}{10}, \tag{13}$$

where $c_k; k = 1, 2, 3$ are the optimal coefficients. Multiplying Eqs. (11)—(13) by the corresponding c_k and taking the sum yields a fifth-order interpolation scheme,

$$\hat{f}_{j+1/2} = \frac{1}{30}f_{j-2} - \frac{13}{60}f_{j-1} + \frac{47}{60}f_j + \frac{27}{60}f_{j+1} - \frac{1}{20}f_{j+2}. \tag{14}$$

The optimal coefficients are replaced by nonlinear weights $(\omega_k, k = 1, 2, 3)$ and the fifth-order WENO scheme is the weighted sum of Eqs. (11)–(13), expressed as

$$\hat{f}_{j+1/2} = \frac{\omega_1}{3}f_{j-2} - \frac{1}{6}(7\omega_1 + \omega_2)f_{j-1} + \frac{1}{6}(11\omega_1 + 5\omega_2 + 2\omega_3)f_j + \frac{1}{6}(2\omega_2 + 5\omega_3)f_{j+1} - \frac{\omega_3}{6}f_{j+2}. \tag{15}$$

The nonlinear weights are evaluated based on the smoothness of the solution,[40]

$$\omega_k = \frac{\alpha_k}{\sum_k \alpha_k};\ \alpha_k = c_k\left[1 + \left(\frac{\tau}{\epsilon + \beta_k}\right)^2\right], \tag{16}$$

where

$$\tau = \left(f_{j-2} - 4f_{j-1} + 6f_j - 4f_{j+1} + f_{j+2}\right)^2. \tag{17}$$

The parameter $\epsilon = 10^{-6}$ prevents division by zero, and the smoothness indicators (β_k) are given by

$$\beta_1 = \frac{13}{12}(f_{j-2} - 2f_{j-1} + f_j^2 + \frac{1}{4}(f_{j-2} - 4f_{j-1} + 3f_j^2, \tag{18}$$

$$\beta_2 = \frac{13}{12}(f_{j-1} - 2f_j + f_{j+1}^2 + \frac{1}{4}(f_{j-1} - f_{j+1}^2, \tag{19}$$

$$\text{and } \beta_3 = \frac{13}{12}(f_j - 2f_{j+1} + f_{j+2}^2 + \frac{1}{4}(3f_j - 4f_{j+1} + f_{j+2}^2. \tag{20}$$

Other definitions for the nonlinear weights exist in the literature,[41,42,43] as well as a comparison of the nonlinear properties of the WENO5 scheme with these weights.[30] When the solution is smooth, the nonlinear weights converge to the optimal coefficients ($\omega_k \to c_k$), and Eq. (15) reduces to Eq. (14). The scheme is fifth-order accurate for such solutions. Across and near discontinuities, the weights corresponding to the stencil containing the discontinuity approach zero, and Eq. (15) represents an interpolation scheme with its stencil biased away from the discontinuity. Nonoscillatory solutions are thus obtained.

The CRWENO schemes are constructed by applying the solution-dependent stencil selection mechanism of the WENO schemes to compact finite-difference schemes. Compact finite-difference schemes are characterized by higher spectral resolution,[29] and the CRWENO schemes yield nonoscillatory solutions with lower dissipation and higher resolution.[28,30,31] The fifth-order CRWENO scheme (CRWENO5)[28] is constructed by considering three third-order accurate compact interpolation schemes for the numerical flux $\hat{f}_{j+1/2}$:

$$\frac{2}{3}\hat{f}^1_{j-1/2} + \frac{1}{3}\hat{f}^1_{j+1/2} = \frac{1}{6}\left(f_{j-1} + 5f_j\right); \qquad c_1 = \frac{2}{10}, \tag{21}$$

$$\frac{1}{3}\hat{f}^2_{j-1/2} + \frac{2}{3}\hat{f}^2_{j+1/2} = \frac{1}{6}\left(5f_j + f_{j+1}\right); \qquad c_2 = \frac{5}{10}, \tag{22}$$

$$\frac{2}{3}\hat{f}^3_{j+1/2} + \frac{1}{3}\hat{f}^3_{j+3/2} = \frac{1}{6}\left(f_j + 5f_{j+1}\right); \qquad c_3 = \frac{3}{10}, \tag{23}$$

where $c_k, k = 1, 2, 3$ are the optimal coefficients. A fifth-order compact scheme is obtained by multiplying Eqs. (22)–(23) by their corresponding optimal coefficient c_k and adding

$$\frac{3}{10}\hat{f}_{j-1/2} + \frac{6}{10}\hat{f}_{j+1/2} + \frac{1}{10}\hat{f}_{j+3/2} = \frac{1}{30}f_{j-1} + \frac{19}{30}f_j + \frac{1}{3}f_{j+1}. \tag{24}$$

The CRWENO5 scheme is constructed by replacing the optimal coefficients c_k by nonlinear weights ω_k and can be expressed as

$$\left(\frac{2}{3}\omega_1 + \frac{1}{3}\omega_2\right)\hat{f}_{j-1/2} + \left[\frac{1}{3}\omega_1 + \frac{2}{3}(\omega_2 + \omega_3)\right]\hat{f}_{j+1/2} + \frac{1}{3}\omega_3\hat{f}_{j+3/2} = \frac{\omega_1}{6}f_{j-1} + \frac{5(\omega_1 + \omega_2) + \omega_3}{6}f_j + \frac{\omega_2 + 5\omega_3}{6}f_{j+1}. \tag{25}$$

The weights ω_k are computed by Eq. (16) and Eqs. (18)–(20). The resulting scheme, Eq. (25), is fifth-order accurate when the solution is smooth ($\omega_k \to c_k$) and reduces to Eq. (24). Across and near discontinuities, the weights corresponding to the stencils containing the discontinuity approach zero, and a biased (away from the discontinuity) compact scheme is obtained. Equation (25) results in a tridiagonal system of equations that must be solved at each time-integration step or stage. An efficient and scalable implementation of the CRWENO5 scheme is proposed in[32,44] and used in this study.

The solution of a hyperbolic system is composed of waves propagating at their characteristic speeds along their characteristic directions. Thus, the final flux at the interface is an appropriate combination of the left- and right-biased fluxes. The Rusanov scheme[45,46] is used and is given by

$$\hat{\mathbf{f}}_{j+1/2} = \frac{1}{2}\left[\hat{\mathbf{f}}^L_{j+1/2} + \hat{\mathbf{f}}^R_{j+1/2} + \max_{j,j+1}\nu_j\left(\hat{\mathbf{q}}^L_{j+1/2} - \hat{\mathbf{q}}^R_{j+1/2}\right)\right], \tag{26}$$

where the superscripts L and R indicate left- and right-biased interpolations, respectively. The dissipation factor is $\nu = a + |\mathbf{u}|$, where a is the speed of sound and $\mathbf{u}$ is the flow velocity. Of note is the fact that $\hat{\mathbf{q}}^{L,R}_{j+1/2}$ are the left- and right-biased interface values for $\mathbf{q}$ that are reconstructed in the same manner as $\hat{\mathbf{f}}^{L,R}_{j+1/2}$.

B. Well-Balanced Formulation

Equation (6) is a hyperbolic balance law with steady-state solutions where the pressure gradient is exactly balanced by the gravitational source term. Atmospheric flows are often small perturbations to this balanced steady state, and the ability to preserve such steady states to round-off errors is critical in ensuring that numerical errors do not overwhelm the physical perturbations. A well-balanced conservative finite-difference algorithm recently was proposed;[35] however, the formulation is limited to an isothermal equilibrium. A general formulation is introduced in this study based on the approach described in[36,47,35] that holds for any hydrostatic equilibrium. Specific examples illustrate the application of this formulation to the equilibria encountered in flow problems of practical relevance. The well-balanced algorithm is described for two-dimensional flows with gravity acting along the y dimension; however, the formulation presented can be easily extended to three dimensions and for domains where the gravity may not be aligned with a specific dimension.

Equation (6) admits steady-state solutions that may be expressed as

$$u = \text{constant}, v = 0,\ \rho = \rho_0 \varrho\left(y\right),\ p = p_0 \varphi\left(y\right), \tag{27}$$

where the subscript 0 indicates the flow variables at a reference altitude. The pressure and density at the reference altitude are related by the equation of state $p_0 = \rho_0 R T_0$. At equilibrium, Eq. (6) reduces to

$$\frac{dp}{dy} = -\rho g. \tag{28}$$

Therefore, by substituting Eq. (27) in Eq. (28) and considering the equation of state, the functions $\varrho\left(y\right)$ and $h\left(y\right)$ satisfy the following relation:

$$R T_0 \left[\varrho\left(y\right)\right]^{-1} \varphi'\left(y\right) = -g. \tag{29}$$

A well-balanced finite-difference method is implemented by modifying Eq. (6) as

$$\frac{\partial \mathbf{q}}{\partial t} + \frac{\partial \mathbf{F}\left(\mathbf{q}\right)}{\partial x} + \frac{\partial \mathbf{G}\left(\mathbf{q}\right)}{\partial y} = \mathbf{s}^*\left(\mathbf{q}, y\right), \tag{30}$$

where $\mathbf{s}^* = \left[0, 0, \rho R T_0 \left[\varrho\left(y\right)\right]^{-1} \varphi'\left(y\right), \rho v R T_0 \left[\varrho\left(y\right)\right]^{-1} \varphi'\left(y\right)\right]^{\mathrm{T}}$. Equation (29) ensures that Eq. (30) is consistent with Eq. (6), rendering the source terms in a form similar to that of the flux term.[36,35] A well-balanced algorithm must satisfy the hydrostatic balance in its discretized form. Thus, the discretized flux derivative must exactly balance the discretized source term. A linear finite-difference approximation to the derivative of a function $\phi\left(x\right)$ can be expressed as

$$\left.\frac{\partial \phi}{\partial x}\right|_{x=x_j} \approx \mathcal{D}\left[\phi\right] \equiv \sum_{k=-m}^{n} \sigma_k^{\mathcal{D}} \phi_{j+k}, \tag{31}$$

where m and n are integers defining the stencil $[j-m, j-m+1, \cdots, j+n-1, j+n]$ of the finite-difference operator $\mathcal{D}$ and where $\sigma_k^{\mathcal{D}}$ are the stencil coefficients. The discretized form of Eq. (30) at steady state is given by

$$\mathcal{D}_{\mathbf{G}}\left[p\right] - \rho R T_0 \left\{\varrho\left(y\right)\right\}^{-1} \mathcal{D}_{\mathbf{s}^*}\left[\varphi\left(y\right)\right] = 0, \tag{32}$$

where $\mathcal{D}_{\mathbf{G}}$ and $\mathcal{D}_{\mathbf{s}^*}$ are the finite-difference operators used to approximate the y derivatives of the flux function $\mathbf{G}$ and the source term $\mathbf{s}^*$, respectively. In general, Eq. (32) will not hold true on a grid with a finite number of points even if $\mathcal{D}_{\mathbf{G}}$ and $\mathcal{D}_{\mathbf{s}^*}$ are both consistent finite-difference operators, and the overall algorithm will not be able to preserve the steady solution. However, this relationship is exactly satisfied if

$$\mathcal{D}_{\mathbf{G}} = \mathcal{D}_{\mathbf{s}^*} = \mathcal{D}. \tag{33}$$

By substituting Eq. (33) and exploiting the linearity of $\mathcal{D}$, the left-hand side of Eq. (32) reduces to

$$\mathcal{D}\left[p - \rho R T_0 \left\{\varrho\left(y\right)\right\}^{-1} \varphi\left(y\right)\right] = \mathcal{D}\left[p_0 \varphi\left(y\right) - \rho_0 \varrho\left(y\right) R T_0 \left\{\varrho\left(y\right)\right\}^{-1} \varphi\left(y\right)\right] = 0. \tag{34}$$

Equation (33) implies that a linear finite-difference algorithm to solve Eq. (30) is well balanced (preserves hydrostatically balanced steady states to round-off error) if the flux derivative and the source terms are discretized by the same linear operator.

The spatial discretization schemes used in this study are nonlinear finite-difference operators, and additional steps are required to construct a well-balanced algorithm. Based on the discussion in the preceding section, the discretization of the flux derivative along y can be summarized as follows:

$$\hat{\mathbf{G}}^{L,R}_{j+1/2} = \mathcal{R}^{L,R}_{\mathbf{G}}\left[\mathbf{G}\right] \equiv \sum_{k=-m}^{n} \hat{\sigma}_k \mathbf{G}_{j+k}, \tag{35}$$

$$\hat{\mathbf{G}}_{j+1/2} = \frac{1}{2}\left[\hat{\mathbf{G}}^{L}_{j+1/2} + \hat{\mathbf{G}}^{R}_{j+1/2} + \max_{j,j+1} \nu_j \left(\hat{\mathbf{q}}^{L}_{j+1/2} - \hat{\mathbf{q}}^{R}_{j+1/2}\right)\right], \tag{36}$$

$$\left.\frac{\partial \mathbf{G}}{\partial y}\right|_{y=y_j} \approx \frac{1}{\Delta y}\left[\hat{\mathbf{G}}_{j+1/2} - \hat{\mathbf{G}}_{j-1/2}\right], \tag{37}$$

where j is the grid index along the y coordinate (the index along the x coordinate is suppressed for convenience of notation), $\mathcal{R}^{L,R}_{\mathbf{G}}$ are the reconstruction operators with m and n defining the stencil bounds, and $\hat{\sigma}_k$ are the coefficients for the stencil points. Equations (15) and (25) (representing the WENO5 and CRWENO5 schemes, respectively) can be represented through this operator. The subscript $\mathbf{G}$ denotes that the nonlinear weights (ω_k) are computed based on $\mathbf{G}\left(\mathbf{q}\right)$. The superscripts L and R denote the left- and right-biased operators respectively.

A well-balanced algorithm requires that the derivative of $\varphi\left(y\right)$ in the source term of Eq. (30) be discretized in the same manner as the flux derivative. This can be summarized as follows:

$$\hat{\boldsymbol{\varphi}}^{L,R}_{j+1/2} = \mathcal{R}^{L,R}_{\mathbf{G}}\left[\boldsymbol{\varphi}\right] \equiv \sum_{k=-m}^{n} \hat{\sigma}_k \boldsymbol{\varphi}_{j+k}, \tag{38}$$

$$\hat{\boldsymbol{\varphi}}_{j+1/2} = \frac{1}{2}\left[\hat{\boldsymbol{\varphi}}^{L}_{j+1/2} + \hat{\boldsymbol{\varphi}}^{R}_{j+1/2}\right], \tag{39}$$

$$\left.\frac{\partial \boldsymbol{\varphi}}{\partial y}\right|_{y=y_j} \approx \frac{1}{\Delta y}\left[\hat{\boldsymbol{\varphi}}_{j+1/2} - \hat{\boldsymbol{\varphi}}_{j-1/2}\right], \tag{40}$$

where the vector $\boldsymbol{\varphi}$ is simply given by $\boldsymbol{\varphi} = \left[0, 0, \varphi\left(y\right), \varphi\left(y\right)\right]^{\mathrm{T}}$. The remaining terms in the source $\mathbf{s}^*$ are evaluated at the cell center j. The interpolation operators in Eqs. (35) and (38) are both $\mathcal{R}_{\mathbf{G}}$; the interface values of both $\mathbf{G}$ and $\boldsymbol{\varphi}$ are computed with the same interpolation operator. This is achieved in the WENO5 and CRWENO5 schemes by calculating the weights based on the smoothness of the flux function $\mathbf{G}\left(\mathbf{q}\right)$, and using these weights to compute the interface values of both $\mathbf{G}$ and $\boldsymbol{\varphi}$ at a given time-integration step or stage.

The final step in the construction of a well-balanced method is the suitable modification of the dissipation term in Eq. (36). The Rusanov upwinding procedure, given by Eq. (36), is modified as follows:

$$\hat{\mathbf{G}}_{j+1/2} = \frac{1}{2}\left[\hat{\mathbf{G}}^{L}_{j+1/2} + \hat{\mathbf{G}}^{R}_{j+1/2} + \kappa \max_{j,j+1} \nu_j \left(\hat{\mathbf{q}}^{*,L}_{j+1/2} - \hat{\mathbf{q}}^{*,R}_{j+1/2}\right)\right], \tag{41}$$

where $\kappa = \max_{j,j+1} \varphi\left(y\right)$, $\hat{\mathbf{q}}^{*,L}_{j+1/2}$ and $\hat{\mathbf{q}}^{*,R}_{j+1/2}$ are the left- and right-biased interpolation (at the interface) of a modified state vector $\mathbf{q}^* = \left[\rho\left\{\varrho\left(y\right)\right\}^{-1}, \rho u\left\{\varrho\left(y\right)\right\}^{-1}, \rho v\left\{\varrho\left(y\right)\right\}^{-1}, e^*\right]^{\mathrm{T}}$. The modified energy e^* is given by

$$e^* = \frac{p\left\{\varphi\left(y\right)\right\}^{-1}}{\gamma - 1} + \frac{1}{2}\rho\left\{\varrho\left(y\right)\right\}^{-1}\left(u^2 + v^2\right). \tag{42}$$

At steady state, $\mathbf{q}^*$ is a constant, and the dissipation term in Eq. (41) is zero with this modification ($\hat{\mathbf{q}}^{*,L}_{j+1/2} = \hat{\mathbf{q}}^{*,R}_{j+1/2}$).

Discretization of the flux derivatives in Eq. (30) by Eqs. (35), (41), and (37) and evaluation of the source term as Eqs. (38), (39), and (40) result in the following form for the steady-state solution given by Eq. (27) at grid point j:

$$p_0\left[\frac{\hat{\varphi}_{j+1/2} - \hat{\varphi}_{j-1/2}}{\Delta y}\right] = \rho_j R T_0 \left\{\varrho(y_j)\right\}^{-1}\left[\frac{\hat{\varphi}_{j+1/2} - \hat{\varphi}_{j-1/2}}{\Delta y}\right], \tag{43}$$

where the $\hat{\varphi}_{j+1/2}$ denotes the interface approximation of the scalar function $\varphi\left(y\right)$. It is evaluated on the left-hand side through Eq. (35) and Eq. (41) and is evaluated on the right-hand side through Eq. (38) and Eq. (39). Equation (43) is exactly satisfied if the operator $\mathcal{R}_{\mathbf{G}}$ is linear. Although $\mathcal{R}_{\mathbf{G}}$ represents nonlinear finite-difference operators Eqs. (15) and (25), the nonlinearity of these schemes arises from the solution-dependent weights ω_k. Within a time-integration step or stage, these weights are computed and fixed, and the operator $\mathcal{R}_{\mathbf{G}}$ is essentially linear. Therefore, Eq. (43) is exactly satisfied.

SUMMARY The steps to construct a well-balanced conservative finite-difference algorithm are summarized as follows:

1. The governing equations are modified as Eq. (30).
2. The flux derivatives are computed through Eqs. (35), (41), and (37).
3. The derivatives in the modified source term are computed through Eqs. (38), (39), and (40) (the remaining terms are evaluated at the cell centers).

The resulting algorithm will preserve a hydrostatically balanced steady state to round-off errors. Three examples of the steady state are presented in the Appendix that are representative of the hydrostatic balance occurring in atmospheric flows.

C. Time Integration

Spatial discretization of Eq. (30) results in a system of ODEs in time,

$$\frac{d\mathbf{q}}{dt} = \mathbf{L}\left(\mathbf{q}\right), \tag{44}$$

where $\mathbf{L}$ denotes the right-hand side operator comprising the discretized flux and source terms. Equation (44) is integrated with multistage explicit Runge-Kutta schemes, expressed as follows:

$$\mathbf{Q}^{(s)} = \mathbf{q}^n + \Delta t \sum_{t=1}^{s-1} a_{st} \mathbf{L}\left(\mathbf{Q}^{(t)}\right), \; s = 1, \cdots, S \tag{45}$$

$$\mathbf{q}^{n+1} = \mathbf{q}^n + \Delta t \sum_{s=1}^{S} b_s \mathbf{L}\left(\mathbf{Q}^{(s)}\right), \tag{46}$$

where S is the number of stages; $\mathbf{Q}^{(s)}$ is the sth stage value; a_{st} and b_s are the coefficients of the Butcher table;[48] and the superscripts n and $n+1$ denote the time levels $t^n = n\Delta t$ and $t^{n+1} = (n+1)\Delta t$, respectively. The strong-stability-preserving third-order Runge-Kutta (SSPRK3)[49] and the classical fourth-order Runge-Kutta (RK4) schemes are used in this study. Their Butcher tables are given by

$$\begin{array}{c|ccc} 0 & 0 & & \\ 1 & 1 & 0 & \\ 1/2 & 1/4 & 1/4 & 0 \\ \hline & 1/6 & 1/6 & 2/3 \end{array}, \quad \text{and} \quad \begin{array}{c|cccc} 0 & 0 & & & \\ 1/2 & 1/2 & 0 & & \\ 1/2 & 0 & 1/2 & 0 & \\ 1 & 0 & 0 & 1 & 0 \\ \hline & 1/6 & 1/3 & 1/3 & 1/6 \end{array}, \tag{47}$$

respectively.

IV. Verification and Results

The numerical method described in the previous section is verified here for several atmospheric flow problems, and its ability to preserve a balanced steady state is demonstrated. Several benchmark problems are solved in order to evaluate the performance and resolution of the proposed algorithm, and the results are compared with those in the literature.

A. Well-Balanced Tests

Three examples of hydrostatic equilibria encountered in atmospheric flows are presented in the Appendix and briefly described below. Here, the ability of the proposed formulation to preserve these equilibria is tested. The initial solution is specified as the steady-state flow. The specific heat ratio is $\gamma = 1.4$ in all the examples.

CASE 1 The first case corresponds to the isothermal equilibrium (Example 1 in the Appendix). The initial solution is specified by Eq. (53) with $u = v = 0.0$, $\rho_0 = 1.21$, $p_0 = 1.0$, and $g = 1.0$. The domain is a unit square discretized by 51×51 points. No-slip wall conditions are specified on all boundaries. This is a nondimensional test case. A time step size of 0.005 is taken, and the solution is evolved until a final time of 10 with the SSPRK3 method.

Table 1. Relative error with respect to the initial solution for the three equilibria with the WENO5 and CRWENO5 schemes.

Case	$\|\epsilon\|_1$	$\|\epsilon\|_2$	$\|\epsilon\|_\infty$	$\|\epsilon\|_1$	$\|\epsilon\|_2$	$\|\epsilon\|_\infty$
	WENO5			CRWENO5		
Case 1	2.46E-15	2.89E-15	3.91E-15	2.00E-14	1.71E-14	1.50E-14
Case 2	6.02E-15	7.11E-15	1.31E-14	1.50E-14	1.53E-14	2.09E-14
Case 3	3.63E-15	4.35E-15	8.15E-15	1.58E-14	1.83E-14	6.11E-14

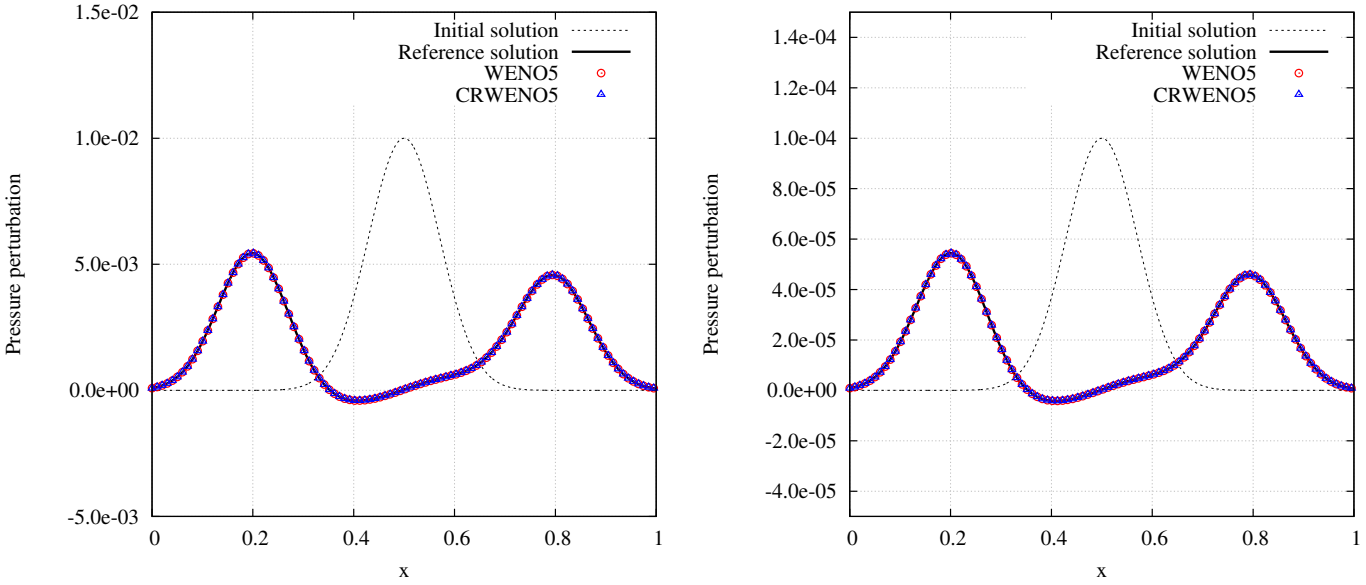

(a) $\eta = 10^{-2}$ (b) $\eta = 10^{-4}$

Figure 1. Pressure perturbation at a final time of 0.25 on a grid with 200 points with the WENO5 and CRWENO5 schemes. The reference solution is obtained with the CRWENO5 scheme on a grid with 2000 points.

Case 2 The second case corresponds to a stratified atmosphere with constant potential temperature θ (Example 2 in the Appendix). The initial solution is specified by Eq. (56) with $u = v = 0$ ms^{-1}, $R = 287.058$ JKg^{-1}K^{-1}, $T = 300$ K, $p_0 = 10^5$ Pa, and $g = 9.8$ ms^{-2}. The domain is 1000×1000 m^2 discretized by 51×51 points. No-slip wall conditions are specified on all boundaries. This case represents the hydrostatic equilibrium for the two-dimensional rising thermal bubble problem.[9] A time step size of 0.02 is taken, and the solution is evolved until a final time of 1000 s with the RK4 method.

Case 3 The third case corresponds to a stratified atmosphere with a specified Brunt-Väisälä frequency $\mathcal{N}$ (Example 3 in the Appendix). The initial solution is specified by Eq. (63) with $\mathcal{N} = 0.01$ s^{-1}, $u = 20$ms^{-1}, $v = 0$ ms^{-1}, $R = 287.058$ JKg^{-1}K^{-1}, $T = 300$ K, $p_0 = 10^5$ Pa, and $g = 9.8$ ms^{-2}. The domain is $300,000 \times 10,000$ m^2 discretized by 1200×50 points. Periodic boundaries are specified along x, and no-slip wall boundaries are specified along y. This case represents the hydrostatic equilibrium for the inertia-gravity wave problem.[9] A time step size of 0.25 is taken, and the solution is evolved until a final time of 3000 s with the SSPRK3 method.

Table 1 shows the L_1, L_2, and L_∞ norms of the difference between the initial and final solutions for the three cases, defined as

$$\|\epsilon\|_{(\cdot)} = \frac{\|\mathbf{q}(\mathbf{x}, t_f) - \mathbf{q}(\mathbf{x}, 0)\|_{(\cdot)}}{\|\mathbf{q}(\mathbf{x}, 0)\|_{(\cdot)}}, \tag{48}$$

where t_f denotes the final time. The differences are zero to machine precision for both the CRWENO5 and WENO5 schemes for all the cases, thus demonstrating that the algorithm accurately preserves the hydrostatic balance.

The ability of the algorithm to simulate small perturbations accurately is demonstrated by considering a one-dimensional

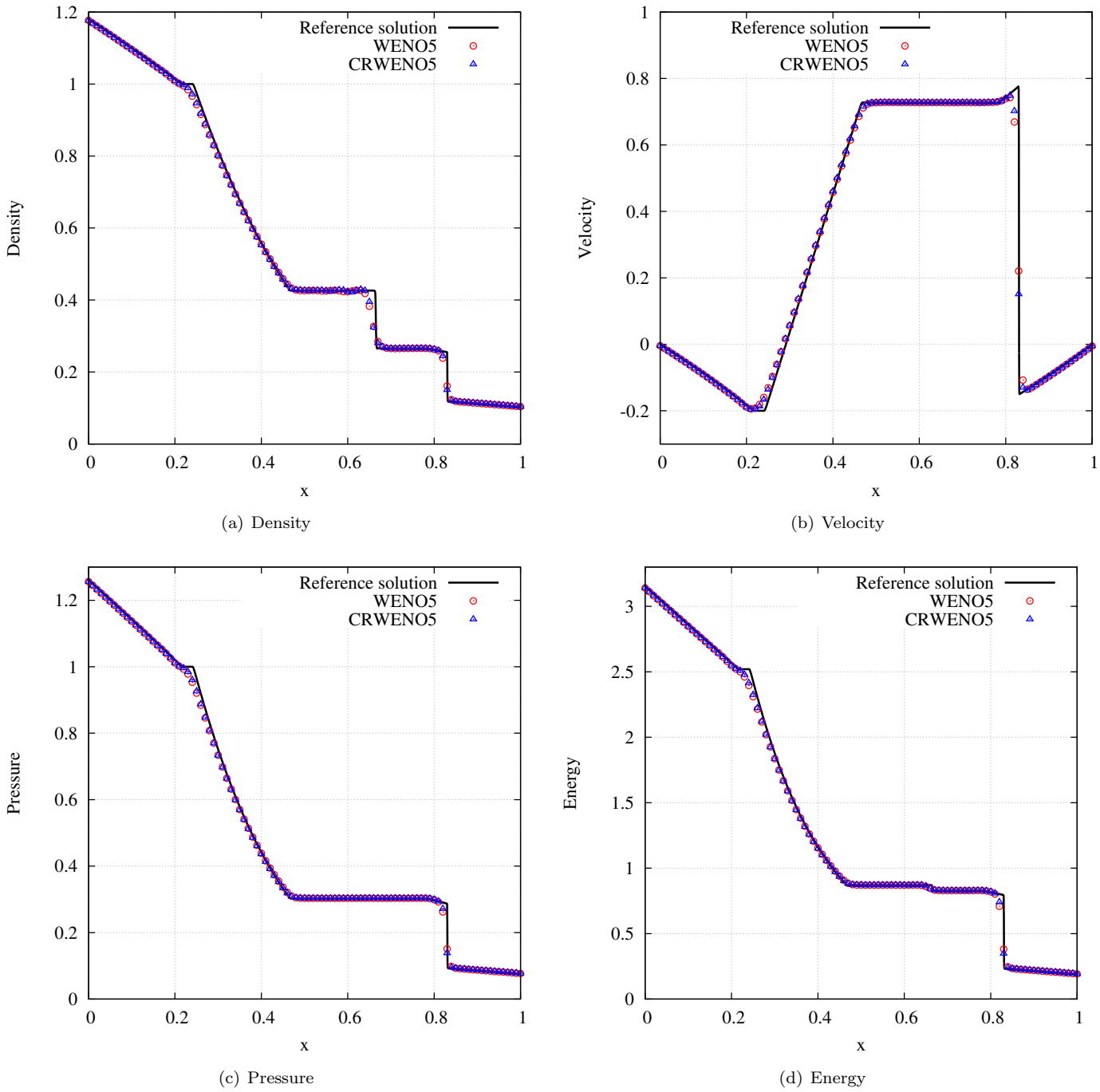

(a) Density (b) Velocity

(c) Pressure (d) Energy

Figure 2. Solution to the modified Sod's shock tube problem (with gravity) obtained with the WENO5 and CRWENO5 scheme on a grid with 101 points. The reference solution is obtained with the CRWENO5 scheme on a grid with 2001 points.

example.[35] The initial solution represents a pressure perturbation to an isothermal hydrostatic equilibrium,

$$\rho(x,0) = \exp(-x), \; p(x,0) = \exp(-x) + \eta \exp\left[-100\,(x-0.5)^2\right], \; u(x,0) = 0, \tag{49}$$

on a unit domain $[0,1]$ with extrapolative boundary conditions. Solutions are obtained at a final time of 0.25 with the RK4 method and a time step size of 0.0025 (corresponding to a CFL of ~ 0.6). Figure 1 shows the initial and final pressure perturbations ($p(x,t) - \exp(-x)$), obtained with the WENO5 and CRWENO5 schemes on a grid with 200 points. The reference solutions are obtained with the CRWENO5 scheme on a grid with 2000 points. Two values of the perturbation strength (η) are considered—10^{-2} and 10^{-4}. The computed solutions agree well with the reference solutions and with

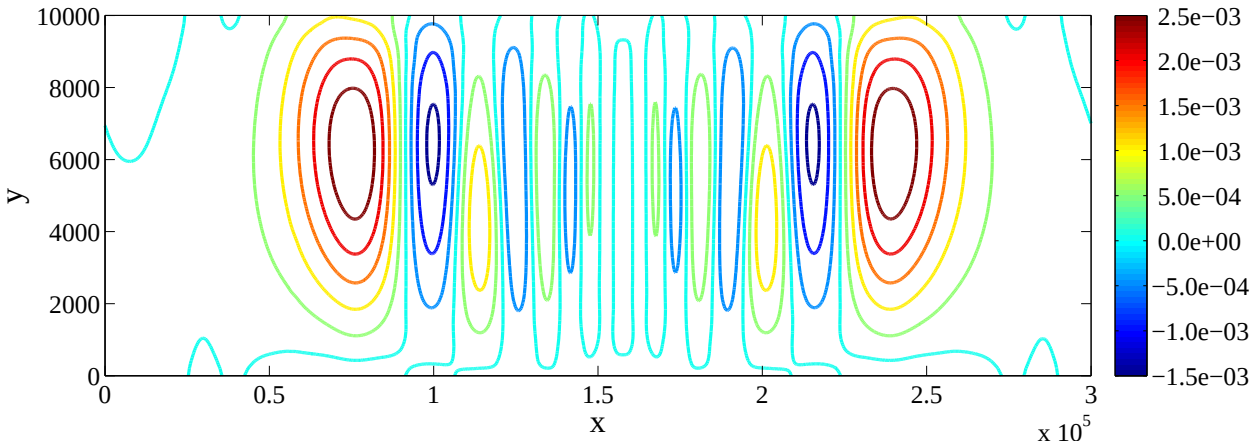

Figure 3. Inertia-gravity waves: Potential temperature perturbation contours for the solution obtained at 3000 s with the CRWENO5 scheme on a grid with 1200×50 points. The contours are plotted from -0.0015 to 0.003 with an interval of 0.0005.

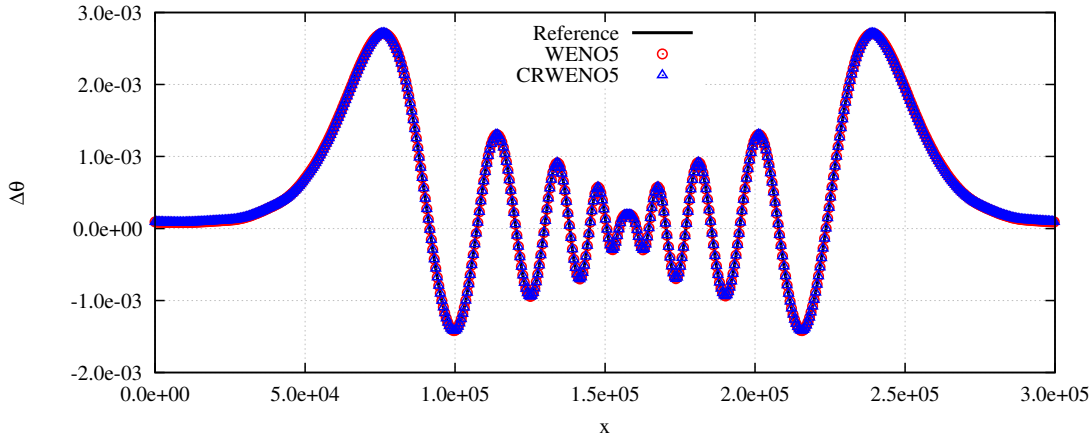

Figure 4. Inertia-gravity waves:Cross-sectional potential temperature perturbation at $y = 5000$ m for the solution obtained at 3000 s with the WENO5 and CRWENO5 scheme on a grid with 1200×50 points (250 m $\times$ 200 m resolution. The reference solution is computed using a spectral element solver[9] with 10th order polynomials and 250 m grid resolution.

results in the literature.[35]

B. Sod's Shock Tube with Gravitational Forcing

The Sod shock tube test[50] is a benchmark one-dimensional Riemann problem. A modified test case with gravitational forcing[35] is solved. The initial solution is given by

$$(\rho, u, p) = \begin{cases} (1, 0, 1) & x < 0.5 \\ (0.125, 0, 0.1) & x \geq 0.5 \end{cases}, \tag{50}$$

on a unit domain $[0, 1]$ discretized by a grid with 101 points. Reflective boundary conditions are applied at both ends of the domain. The flow is subjected to a gravitational field $g = 1$. Solutions are obtained at a final time of 0.2 with the SSPRK3 method and a time step size of 0.002 (corresponding to a CFL of ~ 0.4). Figure 2 shows the solutions obtained with the WENO5 and CRWENO5 scheme. The reference solution is obtained with the CRWENO5 scheme on a grid with 2001 points. The computed solutions agree well with results in the literature.[35]

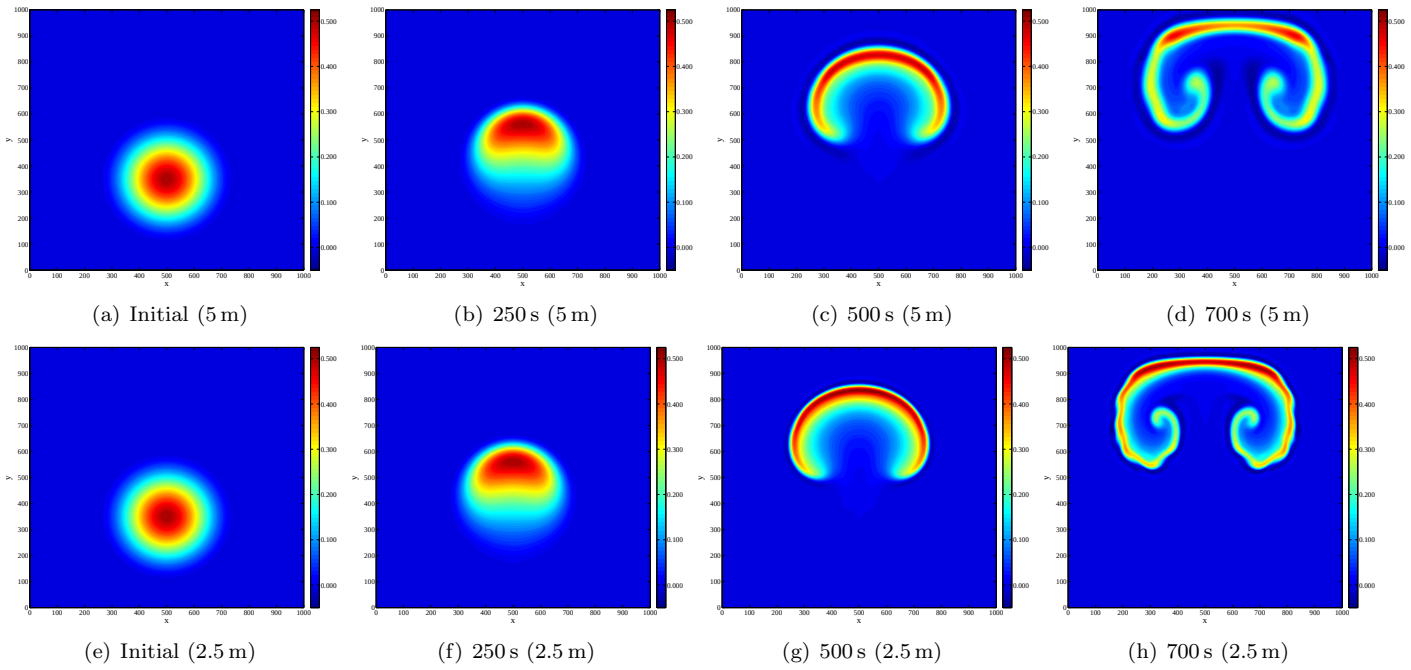

(a) Initial (5 m) (b) 250 s (5 m) (c) 500 s (5 m) (d) 700 s (5 m)

(e) Initial (2.5 m) (f) 250 s (2.5 m) (g) 500 s (2.5 m) (h) 700 s (2.5 m)

Figure 5. Rising thermal bubble: Potential temperature pertubation ($\Delta\theta$) contours for the solution obtained with the WENO5 scheme on grids with 201×201 and 401×401 points (5 m and .25 m resolutions, respectively).

C. Inertia-Gravity Waves

The inertia-gravity wave[51,9] is a two-dimensional benchmark atmospheric flow problem that involves the evolution of a potential temperature perturbation. The domain consists of a channel with dimensions $300,000\,\text{m} \times 10,000\,\text{m}$. Periodic boundary conditions are applied on the left ($x = 0\,\text{m}$) and right ($x = 300,000\,\text{m}$) boundaries, while inviscid wall boundary conditions are applied on the bottom ($y = 0\,\text{m}$) and top ($y = 10,000\,\text{m}$) boundaries. The initial flow is a perturbation added to a stratified atmosphere in hydrostatic balance (Example 3 in the Appendix). The Brunt-Väisälä frequency is specified as $\mathcal{N} = 0.01\,/\text{s}$, the gravitational force per unit mass is $9.8\,\text{m/s}^2$, and the horizontal flow velocity is $u = 20\,\text{m/s}$ throughout the domain. The reference pressure and temperature at $y = 0\,\text{m}$ are $10^5\,\text{N/m}^2$ and 300 K, respectively. The perturbation is added to the potential temperature, specified as

$$\Delta\theta\left(x, y, t = 0\right) = \theta_c \sin\left(\frac{\pi_c y}{h_c}\right)\left[1 + \left(\frac{x - x_c}{a_c}\right)^2\right]^{-1}, \tag{51}$$

where $\theta_c = 0.01\,\text{K}$ is the perturbation strength, $h_c = 10,000\,\text{m}$ is the height of the domain, $a_c = 5,000\,\text{m}$ is the pertubation half-width, $x_c = 100,000\,\text{m}$ is the horizontal location of the perturbation, and $\pi_c \approx 3.141592654$ is the Archimedes (trigonometric) constant. The evolution of the perturbation is simulated until a final time of 3000 s.

Solutions are obtained with the WENO5 and CRWENO5 scheme on a grid with 1200×50 points that results in a resolution of 250 m in x and 200 m in y. The SSPRK3 method is used for time integration with a time step size of 0.25 s (corresponding to a CFL of ~ 0.4). Figure 3 shows the potential temperature perturbation ($\Delta\theta$) at the final time. The initial perturbation is centered at $x = 100,000\,\text{m}$, and the flow features in the final solution are centered at $x = 160,000\,\text{m}$; this translation is expected because of the mean horizontal velocity of 20 m/s. The initial perturbation thus propagates symmetrically to the left and right. Figure 4 shows the cross-sectional potential temperature perturbation at an altitude of $y = 5,000\,\text{m}$. The reference solution is obtained by a spectral-element solver[9] (that solves the governing equations expressed in terms of mass, momentum, and potential temperature as perturbations around the hydrostatically balanced state) using 10th-order polynomials and an effective grid resolution of 250 m. Excellent agreement is observed between the computed solutions and the reference solution, as well as with results in the literature[18,51,21,24]

D. Rising Thermal Bubble

The two-dimensional rising thermal bubble[9] is another benchmark atmospheric flow that simulates the dynamics of a warm bubble. The domain is specified as $(x, y) \in [0, 1000] \times [0, 1000]\,\text{m}^2$ with inviscid wall boundary conditions on all

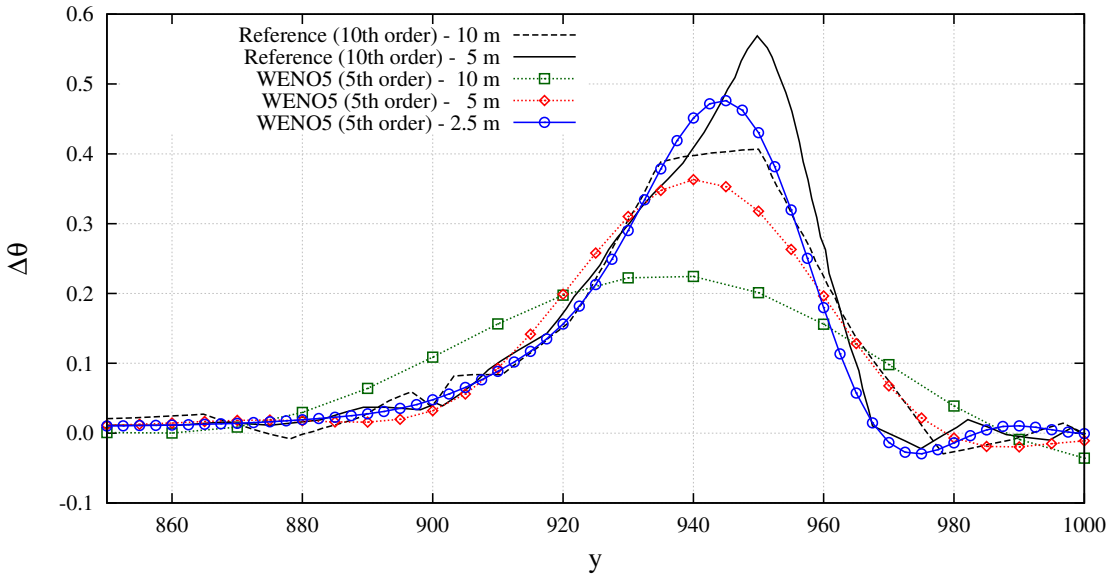

Figure 6. Rising thermal bubble: Cross-sectional potential temperature perturbation ($\Delta\theta$) at $x = 500\,\mathrm{m}$ for the solution obtained at $700\,\mathrm{s}$ with the WENO5 scheme on grids with 101^2, 201^2, and 401^2 points ($10\,\mathrm{m}$, $5\,\mathrm{m}$, and $2.5\,\mathrm{m}$ resolutions, respectively). The reference solutions are computed by using a spectral-element solver[9] with 10th-order polynomials and effective grid resolutions of $5\,\mathrm{m}$ and $10\,\mathrm{m}$.

sides. The initial solution is a stratified atmosphere in hydrostatic balance corresponding to Example 2 in the Appendix. The constant potential temperature (and thus the reference temperature at $y = 0\,\mathrm{m}$) is $300\,\mathrm{K}$, and the reference pressure is $10^5\,\mathrm{N/m^2}$. The ambient flow is at rest and experiences a constant gravitation force per unit mass of $9.8\,\mathrm{m/s^2}$. The warm bubble is added as a potential temperature perturbation, specified as

$$\Delta\theta\,(x, y, t = 0) = \begin{cases} 0 & r > r_c \\ \frac{\theta_c}{2}\left[1 + \cos\left(\frac{\pi_c r}{r_c}\right)\right] & r \le r_c \end{cases}, \quad r = \sqrt{(x - x_c)^2 + (z - z_c)^2}, \tag{52}$$

where $\theta_c = 0.5\,\mathrm{K}$ is the perturbation strength, $(x_c, y_c) = (500, 350)\,\mathrm{m}$ is the initial location at which the bubble is centered, $r_c = 250\,\mathrm{m}$ is the radius of the bubble, and π_c is the trigonometric constant. The flow is simulated to a final of $700\,\mathrm{s}$.

Solutions are obtained with the WENO5 scheme on grids with 101^2, 201^2, and 401^2 points (corresponding to resolutions of $10\,\mathrm{m}$, $5\,\mathrm{m}$, and $2.5\,\mathrm{m}$, respectively). The RK4 method is used for time integration with time step sizes of $0.02\,\mathrm{s}$, $0.01\,\mathrm{s}$, and $0.005\,\mathrm{s}$ (corresponding to a maximum CFL of ~ 0.7). Figure 5 shows the potential temperature perturbation ($\Delta\theta$) for the solutions obtained on grids with 201^2 (Fig. 5(a)–5(d)) and 401^2 points (Fig. 5(e)–5(h)). The solutions are shown at $0\,\mathrm{s}$ (initial bubble), $250\,\mathrm{s}$, $500\,\mathrm{s}$, and $700\,\mathrm{s}$. The warm bubble rises because of buoyancy. The temperature differential within the bubble causes velocity gradients that shear and deform the bubble to a mushroom-like cloud. At the top boundary, the deformed bubble interacts with the inviscid wall to form a thin layer of warm air, while the trailing edges roll up because of the local temperature difference. The solutions obtained on the two grids agree with each other, as well as withe results in the literature.[9,8] The solution obtained on the finer grid is able to resolve small length-scale flow features on the trailing edges.

Figure 6 shows the cross-sectional potential temperature perturbation through $x = 500\,\mathrm{m}$. The numerical solutions obtained by a spectral-element solver[9] (that solves the governing equations with 10th-order polynomial interpolation) are used as a reference. Good agreement is observed. Of note, however, is the fact that although the flow at initial times is smooth, the formation of a thin shear layer requires a nonoscillatory spatial discretization to yield physically relevant solutions. The spectral-element solver applies a spatial filter[9] at the end of each time step to maintain stability; however, nonphysical oscillations remain in the solution, especially at coarse-grid resolution. The WENO5 scheme yields stable solutions, but the solutions are more diffusive compared with the spectral-element solutions, especially on coarse grids.

V. Conclusions

This paper presents a well-balanced conservative finite-difference algorithm for the numerical simulation of atmospheric flows. The governing equations (inviscid Euler equations) are solved as conservation laws for mass, momentum, and energy, with no additional assumptions. The standard conservative finite-difference discretization of the hyperbolic flux and the treatment of the source term are modified so that the overall algorithm preserves hydrostatically balanced equilibria to machine precision. Such precision is essential because atmospheric flows are often small perturbations around the balanced equilibrium and errors in preserving this equilibrium can overwhelm the physically relevant perturbations. This formulation is an extension of previous work by Xing and Shu (2013) to more general flows encountered in atmospheric simulations. The fifth-order weighted essentially nonoscillatory and the compact-reconstruction weighted essentially nonoscillatory schemes are used in this paper for spatial discretization; however, the well-balanced formulation can be used with any conservative finite-difference methods. The ability of the proposed algorithm to preserve the equilibrium flows in hydrostatic balance is demonstrated on three examples of stratified atmosphere commonly encountered. Benchmark flow problems are solved to verify the algorithm, and the results are shown to compare favorably with those in the literature.

Appendix

Three examples of the well-balanced finite-difference formulation are presented. These examples are representative of the hydrostatic equilibrium encountered in benchmark atmospheric flow problems.

Example 1 The first example is the isothermal steady state. The resulting formulation is identical to the previously proposed well-balanced WENO scheme.[35] The steady state can be derived by assuming the temperature $T = T_0$ to be a constant and applying the hydrostatic balance Eq. (28). It is given by

$$u = \text{constant},\ v = 0,\ \rho = \rho_0 \exp\left(-\frac{gy}{RT}\right),\ p = p_0 \exp\left(-\frac{gy}{RT}\right), \tag{53}$$

where the reference density ρ_0 and pressure p_0 are related by the equation of state. Thus, the functions $\varrho(y)$ and $\varphi(y)$ in Eq. (27) are

$$\varrho(y) = \exp\left(-\frac{gy}{RT}\right),\ \varphi(y) = \exp\left(-\frac{gy}{RT}\right). \tag{54}$$

The modified source term in Eq. (30) and the modified solution in Eq. (41) are

$$\mathbf{s}^* = \begin{bmatrix} 0 \\ 0 \\ \rho R T_0 \exp\left(\frac{gy}{RT}\right)\left\{\exp\left(-\frac{gy}{RT}\right)\right\}_y \\ \rho v R T_0 \exp\left(\frac{gy}{RT}\right)\left\{\exp\left(-\frac{gy}{RT}\right)\right\}_y \end{bmatrix}, \text{ and } \mathbf{q}^* = \begin{bmatrix} \rho \exp\left(\frac{gy}{RT}\right) \\ \rho u \exp\left(\frac{gy}{RT}\right) \\ \rho v \exp\left(\frac{gy}{RT}\right) \\ e \exp\left(\frac{gy}{RT}\right) \end{bmatrix}. \tag{55}$$

Example 2 The second example is a hydrostatic balance that is frequently encountered in atmospheric flows of practical relevance.[18,9,10] The steady state is derived by specifying a stratified atmosphere with constant potential temperature $\theta = T_0$. The hydrostatic balance is thus expressed as

$$\frac{\gamma R}{\gamma - 1}\theta \frac{d\pi}{dy} = -g \Rightarrow \rho = \rho_0 \left[1 - \frac{(\gamma-1)gy}{\gamma R \theta}\right]^{1/(\gamma-1)},\ p = p_0 \left[1 - \frac{(\gamma-1)gy}{\gamma R \theta}\right]^{\gamma/(\gamma-1)},\ u = \text{constant},\ v = 0. \tag{56}$$

where π is the Exner pressure (see section II. Thus, the functions $\varrho(y)$ and $\varphi(y)$ in Eq. (27) are

$$\varrho(y) = \left[1 - \frac{(\gamma-1)gy}{\gamma R \theta}\right]^{1/(\gamma-1)},\ \varphi(y) = \left[1 - \frac{(\gamma-1)gy}{\gamma R \theta}\right]^{\gamma/(\gamma-1)}, \tag{57}$$

and the modified source term in Eq. (30) and the modified solution in Eq. (41) are

$$\mathbf{s}^* = \begin{bmatrix} 0 \\ 0 \\ \rho R T_0 \left\{1 - \frac{(\gamma-1)gy}{\gamma R\theta}\right\}^{-1/(\gamma-1)} \left\{\left(1 - \frac{(\gamma-1)gy}{\gamma R\theta}\right)^{\gamma/(\gamma-1)}\right\}_y \\ \rho v R T_0 \left\{1 - \frac{(\gamma-1)gy}{\gamma R\theta}\right\}^{-1/(\gamma-1)} \left\{\left(1 - \frac{(\gamma-1)gy}{\gamma R\theta}\right)^{\gamma/(\gamma-1)}\right\}_y \end{bmatrix}, \tag{58}$$

and

$$\mathbf{q}^* = \begin{bmatrix} \rho\left\{1-\frac{(\gamma-1)gy}{\gamma R\theta}\right\}^{-1/(\gamma-1)} \\ \rho u\left\{1-\frac{(\gamma-1)gy}{\gamma R\theta}\right\}^{-1/(\gamma-1)} \\ \rho v\left\{1-\frac{(\gamma-1)gy}{\gamma R\theta}\right\}^{-1/(\gamma-1)} \\ e^* \end{bmatrix}, \tag{59}$$

where

$$e^* = \frac{p}{\gamma-1}\left[1-\frac{(\gamma-1)gy}{\gamma R\theta}\right]^{-\gamma/(\gamma-1)} + \frac{1}{2}\rho\left[1-\frac{(\gamma-1)gy}{\gamma R\theta}\right]^{-1/(\gamma-1)}\left(u^2+v^2\right). \tag{60}$$

EXAMPLE 3 The third example is a stratified atmosphere with a specified Brunt-Väisälä frequency ($\mathcal{N}$)[51,9]

$$\mathcal{N}^2 = g\frac{d}{dy}\left(\log\theta\right) \Rightarrow \theta = T_0\exp\left(\frac{\mathcal{N}^2}{g}y\right). \tag{61}$$

Assuming hydrostatic balance, the Exner pressure is given by

$$\pi = 1+\frac{(\gamma-1)g^2}{\gamma RT_0\mathcal{N}^2}\left[\exp\left(-\frac{\mathcal{N}^2}{g}y\right)-1\right], \tag{62}$$

and the steady state flow variables are

$$p = p_0\left[1+\frac{(\gamma-1)g^2}{\gamma RT_0\mathcal{N}^2}\left\{\exp\left(-\frac{\mathcal{N}^2}{g}y\right)-1\right\}\right]^{\gamma/(\gamma-1)}, \tag{63}$$

$$\rho = \rho_0\exp\left(-\frac{\mathcal{N}^2}{g}y\right)\left[1+\frac{(\gamma-1)g^2}{\gamma RT_0\mathcal{N}^2}\left\{\exp\left(-\frac{\mathcal{N}^2}{g}y\right)-1\right\}\right]^{1/(\gamma-1)}, \tag{64}$$

$$u = \text{constant},\ v=0. \tag{65}$$

Thus, the functions $\varrho\left(y\right)$ and $\varphi\left(y\right)$ in Eq. (27) are

$$\varrho\left(y\right) = \exp\left(-\frac{\mathcal{N}^2}{g}y\right)\left[1+\frac{(\gamma-1)g^2}{\gamma RT_0\mathcal{N}^2}\left\{\exp\left(-\frac{\mathcal{N}^2}{g}y\right)-1\right\}\right]^{1/(\gamma-1)}, \tag{66}$$

$$\varphi\left(y\right) = \left[1+\frac{(\gamma-1)g^2}{\gamma RT_0\mathcal{N}^2}\left\{\exp\left(-\frac{\mathcal{N}^2}{g}y\right)-1\right\}\right]^{\gamma/(\gamma-1)}. \tag{67}$$

The modified source term in Eq. (30) and the modified solution in Eq. (41) are

$$\mathbf{s}^* = \begin{bmatrix} 0 \\ 0 \\ \rho RT_0\exp\left(\frac{\mathcal{N}^2}{g}y\right)\left[1+\frac{(\gamma-1)g^2}{\gamma RT_0\mathcal{N}^2}\left\{\exp\left(-\frac{\mathcal{N}^2}{g}y\right)-1\right\}\right]^{-1/(\gamma-1)}\left\{\left(1+\frac{(\gamma-1)g^2}{\gamma RT_0\mathcal{N}^2}\left\{\exp\left(-\frac{\mathcal{N}^2}{g}y\right)-1\right\}\right)^{\gamma/(\gamma-1)}\right\}_y \\ \rho vRT_0\exp\left(\frac{\mathcal{N}^2}{g}y\right)\left[1+\frac{(\gamma-1)g^2}{\gamma RT_0\mathcal{N}^2}\left\{\exp\left(-\frac{\mathcal{N}^2}{g}y\right)-1\right\}\right]^{-1/(\gamma-1)}\left\{\left(1+\frac{(\gamma-1)g^2}{\gamma RT_0\mathcal{N}^2}\left\{\exp\left(-\frac{\mathcal{N}^2}{g}y\right)-1\right\}\right)^{\gamma/(\gamma-1)}\right\}_y \end{bmatrix} \tag{68}$$

and

$$\mathbf{q}^* = \begin{bmatrix} \rho\exp\left(\frac{\mathcal{N}^2}{g}y\right)\left[1+\frac{(\gamma-1)g^2}{\gamma RT_0\mathcal{N}^2}\left\{\exp\left(-\frac{\mathcal{N}^2}{g}y\right)-1\right\}\right]^{-1/(\gamma-1)} \\ \rho u\exp\left(\frac{\mathcal{N}^2}{g}y\right)\left[1+\frac{(\gamma-1)g^2}{\gamma RT_0\mathcal{N}^2}\left\{\exp\left(-\frac{\mathcal{N}^2}{g}y\right)-1\right\}\right]^{-1/(\gamma-1)} \\ \rho v\exp\left(\frac{\mathcal{N}^2}{g}y\right)\left[1+\frac{(\gamma-1)g^2}{\gamma RT_0\mathcal{N}^2}\left\{\exp\left(-\frac{\mathcal{N}^2}{g}y\right)-1\right\}\right]^{-1/(\gamma-1)} \\ e^* \end{bmatrix}, \tag{69}$$

where

$$e^* = \frac{p}{\gamma-1}\left[1+\frac{(\gamma-1)g^2}{\gamma RT_0\mathcal{N}^2}\left\{\exp\left(-\frac{\mathcal{N}^2}{g}y\right)-1\right\}\right]^{-\gamma/(\gamma-1)} \tag{70}$$

$$+\frac{1}{2}\rho\exp\left(\frac{\mathcal{N}^2}{g}y\right)\left[1+\frac{(\gamma-1)g^2}{\gamma RT_0\mathcal{N}^2}\left\{\exp\left(-\frac{\mathcal{N}^2}{g}y\right)-1\right\}\right]^{-1/(\gamma-1)}\left(u^2+v^2\right). \tag{71}$$

Acknowledgments

This material is based upon work supported by the U.S. Department of Energy, Office of Science, Advanced Scientific Computing Research, under contract DE-AC02-06CH11357.

References

[1]Taylor, M. A., Edwards, J., and Cyr, A. S., "Petascale atmospheric models for the Community Climate System Model: new developments and evaluation of scalable dynamical cores," *Journal of Physics: Conference Series*, Vol. 125, No. 1, 2008, pp. 012023.

[2]Lin, S.-J., "A "vertically Lagrangian" finite-volume dynamical core for global models," *Monthly Weather Review*, Vol. 132, No. 10, 2004, pp. 2293–2307.

[3]Ogura, Y. and Phillips, N., "Scale analysis of deep and shallow convection in the atmosphere," *Journal of the Atmospheric Sciences*, Vol. 19, No. 2, 1962, pp. 173–79.

[4]Durran, D., "Improving the anelastic approximation," *Journal of the Atmospheric Sciences*, Vol. 46, No. 11, 1989, pp. 1453–1461.

[5]Arakawa, A. and Konor, C., "Unification of the anelastic and quasi-hydrostatic systems of equations," *Monthly Weather Review*, Vol. 137, No. 2, 2009, pp. 710–726.

[6]Davies, T., Staniforth, A., Wood, N., and Thuburn, J., "Validity of anelastic and other equation sets as inferred from normal-mode analysis," *Quarterly Journal of the Royal Meteorological Society*, Vol. 129, No. 593, 2003, pp. 2761–2775.

[7]Klein, R., Achatz, U., Bresch, D., Knio, O., and Smolarkiewicz, P., "Regime of validity of soundproof atmospheric flow models," *Journal of the Atmospheric Sciences*, Vol. 67, No. 10, 2010, pp. 3226–3237.

[8]Ullrich, P. and Jablonowski, C., "Operator-split Runge-Kutta-Rosenbrock methods for nonhydrostatic atmospheric models," *Monthly Weather Review*, Vol. 140, No. 4, 2012, pp. 1257–1284.

[9]Giraldo, F. and Restelli, M., "A study of spectral element and discontinuous Galerkin methods for the Navier-Stokes equations in nonhydrostatic mesoscale atmospheric modeling: Equation sets and test cases," *Journal of Computational Physics*, Vol. 227, No. 8, 2008, pp. 3849–3877.

[10]Giraldo, F., Restelli, M., and Läuter, M., "Semi-Implicit Formulations of the Navier-Stokes Equations: Application to Nonhydrostatic Atmospheric Modeling," *SIAM Journal on Scientific Computing*, Vol. 32, No. 6, 2010, pp. 3394–3425.

[11]Grell, G., Dudhia, J., Stauffer, D., et al., "A description of the fifth-generation Penn State/NCAR mesoscale model (MM5)," Tech. rep., 1994.

[12]Hodur, R., "The Naval Research Laboratory's coupled ocean/atmosphere mesoscale prediction system (COAMPS)," *Monthly Weather Review*, Vol. 125, No. 7, 1997, pp. 1414–1430.

[13]Xue, M., Droegemeier, K. K., and Wong, V., "The Advanced Regional Prediction System (ARPS) – A multi-scale nonhydrostatic atmospheric simulation and prediction model. Part I: Model dynamics and verification," *Meteorology and Atmospheric Physics*, Vol. 75, No. 3-4, 2000, pp. 161–193.

[14]Janjic, Z., "A nonhydrostatic model based on a new approach," *Meteorology and Atmospheric Physics*, Vol. 82, No. 1-4, 2003, pp. 271–285.

[15]Gassmann, A., "An improved two-time-level split-explicit integration scheme for non-hydrostatic compressible models," *Meteorology and Atmospheric Physics*, Vol. 88, No. 1-2, 2005, pp. 23–38.

[16]Das, P., "A non-Archimedean approach to the equations of convection dynamics," *Journal of the Atmospheric Sciences*, Vol. 36, No. 11, 1979, pp. 2183–2190.

[17]Skamarock, W. C., Klemp, J. B., Dudhia, J., Gill, D. O., Barker, D. M., Wang, W., and Powers, J. G., "A description of the advanced research WRF version 2," Tech. rep., DTIC Document, 2005.

[18]Ahmad, N. and Lindeman, J., "Euler solutions using flux-based wave decomposition," *International Journal for Numerical Methods in Fluids*, Vol. 54, No. 1, 2007, pp. 47–72.

[19]Botta, N., Klein, R., Langenberg, S., and Lützenkirchen, S., "Well balanced finite volume methods for nearly hydrostatic flows," *Journal of Computational Physics*, Vol. 196, No. 2, 2004, pp. 539–565.

[20]Ahmad, N., Bacon, D., Sarma, A., Koračin, D., Vellore, R., Boybeyi, Z., and Lindeman, J., "Simulations of Non-hydrostatic Atmosphere using Conservation Laws Package," *45th AIAA Aerospace Sciences Meeting and Exhibit, Reno, NV*, American Institute of Aeronautics and Astronautics, 2007.

[21]Ahmad, N. and Proctor, F., "The High-Resolution Wave-Propagation Method Applied to Meso- and Micro-scale Flows," *50th AIAA Aerospace Sciences Meeting and Exhibit, Nashville, TN*, American Institute of Aeronautics and Astronautics, 2012.

[22]Davies, T., Cullen, M. J. P., Malcolm, A. J., Mawson, M. H., Staniforth, A., White, A. A., and Wood, N., "A new dynamical core for the Met Office's global and regional modelling of the atmosphere," *Quarterly Journal of the Royal Meteorological Society*, Vol. 131, No. 608, 2005, pp. 1759–1782.

[23]Kelly, J. F. and Giraldo, F. X., "Continuous and discontinuous Galerkin methods for a scalable three-dimensional nonhydrostatic atmospheric model: Limited-area mode," *Journal of Computational Physics*, Vol. 231, No. 24, 2012, pp. 7988–8008.

[24]Yang, C. and Cai, X., "A Scalable Fully Implicit Compressible Euler Solver for Mesoscale Nonhydrostatic Simulation of Atmospheric Flows," *SIAM Journal on Scientific Computing*, Vol. 36, No. 5, 2014, pp. S23–S47.

[25]Liu, X.-D., Osher, S., and Chan, T., "Weighted Essentially Non-oscillatory Schemes," *Journal of Computational Physics*, Vol. 115, No. 1, 1994, pp. 200–212.

[26]Jiang, G.-S. and Shu, C.-W., "Efficient Implementation of Weighted ENO Schemes," *Journal of Computational Physics*, Vol. 126, No. 1, 1996, pp. 202–228.

[27]Shu, C.-W., "High Order Weighted Essentially Nonoscillatory Schemes for Convection Dominated Problems," *SIAM Review*, Vol. 51, No. 1, 2009, pp. 82–126.

[28]Ghosh, D. and Baeder, J. D., "Compact Reconstruction Schemes with Weighted ENO Limiting for Hyperbolic Conservation Laws," *SIAM Journal on Scientific Computing*, Vol. 34, No. 3, 2012, pp. A1678–A1706.

[29]Lele, S. K., "Compact finite difference schemes with spectral-like resolution," *Journal of Computational Physics*, Vol. 103, No. 1, 1992, pp. 16–42.

[30]Ghosh, D. and Baeder, J. D., "Weighted Non-Linear Compact Schemes for the Direct Numerical Simulation of Compressible, Turbulent Flows," *Journal of Scientific Computing*, Vol. 61, No. 1, October 2014, pp. 61–89.

[31]Ghosh, D., Medida, S., and Baeder, J. D., "Application of Compact-Reconstruction Weighted Essentially Nonoscillatory Schemes to Compressible Aerodynamic Flows," *AIAA Journal*, Vol. 52, No. 9, 2014, pp. 1858–1870.

[32]Ghosh, D., Constantinescu, E. M., and Brown, J., "Efficient Implementation of Nonlinear Compact Schemes on Massively Parallel Platforms," *SIAM Journal on Scientific Computing*, Accepted.

[33]LeVeque, R. J., "Balancing Source Terms and Flux Gradients in High-Resolution Godunov Methods: The Quasi-Steady Wave-Propagation Algorithm," *Journal of Computational Physics*, Vol. 146, No. 1, 1998, pp. 346–365.

[34]Bale, D., LeVeque, R., Mitran, S., and Rossmanith, J., "A Wave Propagation Method for Conservation Laws and Balance Laws with Spatially Varying Flux Functions," *SIAM Journal on Scientific Computing*, Vol. 24, No. 3, 2003, pp. 955–978.

[35]Xing, Y. and Shu, C.-W., "High Order Well-Balanced WENO Scheme for the Gas Dynamics Equations Under Gravitational Fields," *Journal of Scientific Computing*, Vol. 54, No. 2-3, 2013, pp. 645–662.

[36]Xing, Y. and Shu, C.-W., "High-Order Well-Balanced Finite Difference WENO Schemes for a Class of Hyperbolic Systems with Source Terms," *Journal of Scientific Computing*, Vol. 27, No. 1-3, 2006, pp. 477–494.

[37]Laney, C. B., *Computational Gasdynamics*, Cambridge University Press, 1998.

[38]Shu, C.-W. and Osher, S., "Efficient implementation of essentially non-oscillatory shock-capturing schemes," *Journal of Computational Physics*, Vol. 77, No. 2, 1988, pp. 439–471.

[39]Shu, C.-W. and Osher, S., "Efficient implementation of essentially non-oscillatory shock-capturing schemes, II," *Journal of Computational Physics*, Vol. 83, No. 1, 1989, pp. 32–78.

[40]Yamaleev, N. K. and Carpenter, M. H., "A systematic methodology for constructing high-order energy stable WENO schemes," *Journal of Computational Physics*, Vol. 228, No. 11, 2009, pp. 4248–4272.

[41]Henrick, A. K., Aslam, T. D., and Powers, J. M., "Mapped weighted essentially non-oscillatory schemes: Achieving optimal order near critical points," *Journal of Computational Physics*, Vol. 207, No. 2, 2005, pp. 542–567.

[42]Borges, R., Carmona, M., Costa, B., and Don, W. S., "An improved weighted essentially non-oscillatory scheme for hyperbolic conservation laws," *Journal of Computational Physics*, Vol. 227, No. 6, 2008, pp. 3191–3211.

[43]Castro, M., Costa, B., and Don, W. S., "High order weighted essentially non-oscillatory WENO-Z schemes for hyperbolic conservation laws," *Journal of Computational Physics*, Vol. 230, No. 5, 2011, pp. 1766–1792.

[44]Ghosh, D., Constantinescu, E. M., and Brown, J., "Scalable Nonlinear Compact Schemes," Tech. Rep. ANL/MCS-TM-340, Argonne National Laboratory, Argonne, IL, April 2014.

[45]Rusanov, V. V., "The calculation of the interaction of non-stationary shock waves and obstacles," *USSR Computational Mathematics and Mathematical Physics*, Vol. 1, No. 2, 1962, pp. 304–320.

[46]LeVeque, R. J., *Finite Volume Methods for Hyperbolic Problems*, Cambridge Texts in Applied Mathematics, Cambridge University Press, 2002.

[47]Xing, Y. and Shu, C.-W., "High order well-balanced finite volume WENO schemes and discontinuous Galerkin methods for a class of hyperbolic systems with source terms," *Journal of Computational Physics*, Vol. 214, No. 2, 2006, pp. 567–598.

[48]Butcher, J., *Numerical Methods for Ordinary Differential Equations*, Wiley, 2003.

[49]Gottlieb, S., Ketcheson, D. I., and Shu, C.-W., "High Order Strong Stability Preserving Time Discretizations," *Journal of Scientific Computing*, Vol. 38, No. 3, 2009, pp. 251–289.

[50]Sod, G. A., "A survey of several finite difference methods for systems of nonlinear hyperbolic conservation laws," *Journal of Computational Physics*, Vol. 27, No. 1, 1978, pp. 1 – 31.

[51]Skamarock, W. C. and Klemp, J. B., "Efficiency and accuracy of the Klemp-Wilhelmson time-splitting technique," *Monthly Weather Review*, Vol. 122, 1994, pp. 2623–2630.